Published in final edited form as:
IEEE Trans Med Imaging. 2017 August ; 36(8): 1607–1614. doi:10.1109/TMI.2017.2671839.

Novel MRI Technique Enables Non-Invasive Measurement of Atrial Wall Thickness

Marta Varela, **Ross Morgan**, **Adeline Theron**, **Desmond Dillon-Murphy**, **Henry Chubb**, **John Whitaker**, **Markus Henningsson**, **Paul Aljabar**, **Tobias Schaeffter**, **Christoph Kolbitsch**, and **Oleg V. Aslanidi**

Abstract

Knowledge of atrial wall thickness (AWT) has the potential to provide important information for patient stratification and the planning of interventions in atrial arrhythmias. To date, information about AWT has only been acquired in post-mortem or poor-contrast CT studies, providing limited coverage and highly variable estimates of AWT. We present a novel contrast agent-free MRI sequence for imaging AWT and use it to create personalized AWT maps and a biatrial atlas. A novel black-blood phase-sensitive inversion recovery protocol was used to image 10 volunteers and, as proof of concept, 2 atrial fibrillation patients. Both atria were manually segmented to create subject-specific AWT maps using an average of nearest neighbors approach. These were then registered non-linearly to generate an AWT atlas. Atrial wall thickness was 2.4 ± 0.7 and 2.7 ± 0.7 mm in the left and right atria, respectively, in good agreement with post-mortem and CT data, where available. AWT was 2.6 ± 0.7 mm in the left atrium of a patient without structural heart disease, similar to that of volunteers. In a patient with structural heart disease the AWT was increased to 3.1 ± 1.3 mm. We successfully designed an MRI protocol to non-invasively measure AWT and create the first whole-atria AWT atlas. The atlas can be used as a reference to study alterations in thickness caused by atrial pathology. The protocol can be used to acquire personalized AWT maps in a clinical setting and assist in the treatment of atrial arrhythmias.

Index Terms

Atrial wall thickness; atrial fibrillation; catheter ablation; atrial imaging; black-blood MRI; atrial atlas

I Introduction

Information about heart structure is important for understanding cardiac function both in health and disease. Whereas the ventricular wall is routinely imaged for clinical procedure guidance, imaging of the thinner atrial walls remains a major challenge. Atrial wall thickness (AWT) measurements have the potential to provide important clinical information, namely in the assessment of progressive changes in atrial structure linked with atrial arrhythmias [1]. Furthermore, detailed knowledge of AWT may improve both the safety and the efficacy of catheter ablation procedures for atrial tachycardias (AT) and atrial fibrillation (AF), some of the most prevalent cardiovascular diseases in the developed world [2].

Europe PMC Funders Author Manuscripts

Europe PMC Funders Author Manuscripts

Catheter ablation creates localized thermal injury in the atrial wall with the aim of isolating atrial regions where the abnormal electrical activity responsible for arrhythmias resides. Although catheter ablation is one of the first-line treatments for AF, it suffers from recurrence rates as high as 48%-65% [3]. A significant reason is believed to be insufficient energy delivery to create truly transmural lesions at the index procedure, leading to the electrical reconnection of ablated atrial tissue [3]. Excessive energy delivery, however, can cause thermal injury to neighboring structures, leading to complications such as tamponade or esophageal ulceration [3]. There are currently no definitive guidelines for energy deposition in catheter ablation procedures. Detailed pre-procedural AWT maps could help select optimal energy levels for catheter ablations, potentially improving efficacy and safety.

Furthermore, recent studies have highlighted the contribution of AWT to the dynamics of the rotors that can drive AF, suggesting that rotors tend to stabilize in regions of high AWT gradient [4]. Thicker LA regions have also been empirically correlated with complex fractionated electrograms [5]. AWT maps could therefore play a role in the selection of regions where rotors are most likely to reside and which could lead to termination of AF when successfully targeted in ablation procedures.

Increases in wall thickness have additionally been associated with alterations in local mechanical properties, such as reductions in wall stress and longitudinal and radial strain [6]. Finally, AWT maps could help characterize organ-level alterations caused by atrial arrhythmias, aiding in the stratification of AF patients [7].

To date, few studies have focused on measuring the thickness of the atrial wall in either healthy volunteers or patients. Until recently, AWT estimates were performed exclusively in post-mortem studies [8]–[18], sometimes with the aid of histological analysis. This approach is intrinsically limited in terms of spatial coverage, provides thickness measurements which are highly dependent on the direction of the sectioning and raises questions about tissue alterations caused by post-mortem handling. It has provided very variable estimates of AWT, ranging from 1.1 to 6.5 mm in the posterior left atrium (LA) [10], [11].

More recently, AWT has been estimated using computed tomography (CT) images [19]–[28]. Despite its high spatial resolution, CT's inherently poor soft tissue contrast makes the detection of atrial borders very challenging. Although the contrast across the endocardial border can be enhanced with the use of iodine-based contrast agents, the epicardial border remains difficult to identify. Furthermore, to date, all CT studies but one [28] have mimicked anatomical studies, in that AWT is only measured at a low number of discrete locations.

Magnetic Resonance Imaging (MRI)-based studies have so far not been used to measure the thickness of the atrial wall, despite MRI's non-invasiveness and superior soft tissue contrast compared to CT. Bright-blood MRI sequences such as the widely-used balanced steady-state free precession (bSSFP) have an excellent contrast between blood and myocardium, but have a very poor contrast across the epicardial border. Black-blood sequences typically offer better contrast between both blood and myocardium and myocardium and surrounding tissues such as lung and are commonly used for coronary wall imaging. Cardiac black-blood

Europe PMC Funders Author Manuscripts

scans are nevertheless usually performed in 2D or over a small 3D field, due to the difficulty of nulling blood effectively over a large volume of the heart.

In this study, we propose a high-resolution contrast agent-free 3D technique based on an inversion recovery (IR) sequence, more specifically, a phase-sensitive inversion recovery (PSIR) protocol to create high-resolution black-blood MR images. These show a good contrast between blood (which is effectively inverted to have low signal throughout), atrial myocardium (high signal) and extra-cardiac tissues such as lung (intermediate signal). PSIR was initially proposed by Kellman and co-workers to improve the contrast between healthy and infarcted myocardium [29]. In brief, by appending a low contrast reference image at the end of a 2-cardiac beat IR sequence, PSIR allows image phase to be estimated on a voxel-by-voxel basis to give real, rather than magnitude, IR images. This leads to an improvement in contrast between tissues whose signal has a different sign at the chosen inversion time (TI) and, as a consequence, allows for good contrast to be preserved at a larger range of TIs. As the estimated phase image also includes contributions from B_0 inhomogeneities and surface coil sensitivity, PSIR has the added benefit of reducing signal variation caused by these effects.

In this study, we acquire black-blood PSIR images of the left and right atria in 10 healthy volunteers. Each of these images is manually segmented to create meshes of the epi- and endocardial surfaces, from which AWT maps are computed. Using non-linear registration, the AWT maps from volunteers are combined to create an atlas of AWT. To illustrate the application of this workflow in a clinical setting, we also apply it to reconstruct left atrial AWT maps in two AF patients cardioverted to sinus rhythm before ablation therapy. Finally, AWT estimates are compared to literature values from post-mortem and CT studies in the regions where these are available. A diagram of the workflow performed in this study is shown in Fig. 1.

II Methods

A Imaging of Volunteers

10 healthy subjects (3 female, 21-30 years old) were imaged in a Philips 3T Achieva scanner, using a 32-channel cardiac coil. Images were acquired in a para-axial plane using a PSIR sequence with a 3D FLASH readout, typical field-of-view (FOV): 280 x 190 x 120 mm, isotropic-1.40 mm acquisition resolution, flip angle: 20° (5° for the PSIR reference image); echo/repetition times: 2.7/5.9 ms; SENSE factor: 1.5; fat suppression using SPIR. Cardiac triggering was performed just before atrial systole, which was identified from the visual inspection of a 4-chamber CINE image, as is commonly done in the clinical setting. The chosen trigger delay (TD) corresponded to typically 600-750 ms, depending on the subject's heart rate (55-75 bpm on average). An adiabatic non-selective inversion pulse was applied at the longest possible TI that could be accommodated in the volunteer's cardiac cycle, typically 15 ms shorter than the TD (Fig. 2a). This aimed to bring the TI as close as possible to the null time of blood in order to improve blood-myocardium contrast.

Respiratory gating was used, with a pencil-beam navigator placed perpendicularly to the superior border of the liver, giving an average scan time (assuming a 100% breathing

efficiency) of 10 min. Real scan time ranged from 13 to 23 min. A diagram of the pulse sequence is shown in Fig. 2a.

B Imaging of Patients

To prove the feasibility of the proposed technique in patients with AF, AWT was also measured in the LA of 2 AF patients who were in sinus rhythm at the time of the scan (approx. 60 bpm) using the same imaging technique as for volunteers. Main patient characteristics are listed in Table 1.

For clinical reasons, there are some differences in scanning protocol between volunteers and patients (see Fig. 2b). For the patients, imaging was performed at 1.5 T, as this is the field strength at which clinical scans for AF patients are performed locally. Furthermore, due to constraints in scan time, only data for the left atrium was acquired (mean scan time in patients assuming a 100% breathing efficiency: 6 min; real scan time: 9-15 min; typical FOV: 280 x 90 x 120 mm, isotropic 1.4-mm resolution as in the volunteer scans). In the imaged patients, data was acquired at maximal atrial volume, immediately prior to ventricular relaxation, as this was found to be the phase of the cardiac cycle where the atria were still for the longest period. This occurred 200-400 ms after the R-wave, a TI too short to obtain a good myocardium-blood contrast. Scanning was therefore triggered by the pulse peak detected with a peripheral pulse unit (PPU) placed on the subject's finger. This allowed TI to fall in the 600-750 ms range for these patients, giving good blood-myocardium contrast. Finally, for the patients the inversion pulse was immediately preceded by a magnetization transfer contrast pre-pulse, which partially saturated the signal from the myocardium. This was found to lead to a slightly improved discrimination between myocardium and blood at 1.5T. The used pulse sequence is depicted in Fig. 2b.

All imaging was performed under ethical approval (IRAS ID: 171620, 191164), following written informed consent.

C Image Processing

Atrial epicardial and endocardial surfaces were manually segmented by 4 different operators, taking all three imaging planes into consideration, using ITK- SNAP [30] and Seg3D [31]. In some slices, it was not possible to determine the border between the left atrium wall and the aortic root wall. In these instances, the entire border between the LA and the aortic root was included, as introducing such a separation in this region would be highly subjective (see Fig. 3b).

The segmentation of the whole atria was performed in most instances by segmenting along consecutive axial planes, whilst ensuring consistency along the sagittal and coronal planes. To minimize sharp edges between different axial planes, isotropic Gaussian smoothing (σ = 0.2 voxels) was performed after manual segmentation using 3D Slicer [32].

To gauge the reproducibility of the segmentations, a 5^{th} operator blindly repeated the segmentations of the LA of 4 random subjects (2 volunteers and 2 patients). Dice coefficients and 50%-percentile modified Hausdorff distances [33] for endo- and epicardial surfaces were computed as metrics of the inter-operator reproducibility of the segmentations.

Europe PMC Funders Author Manuscripts

The pulmonary vein sleeves and the inferior part of the LA just superior to the mitral valve were not included in these calculations. This is due to the difficulty in objectively determining the extent of the myocardial sleeve of the pulmonary veins or the boundary between the LA and the left ventricle in medical images, as has been noted before [34].

D Thickness Measurements

Triangular meshes of each of the atrial surfaces were generated in Matlab (Mathworks, Natick, MA, USA) using a marching cubes algorithm and resampled to improve mesh quality using MeshLab (Visual Computing Lab, CNR). Each triangular mesh was composed of (mean ± standard deviation) 10022 ± 823 vertices, with internode distance 0.96 ± 0.03 mm. In one randomly chosen subject, we resampled the left atrial mesh more finely (internode distance 0.53 ± 0.02 mm) to evaluate the impact of the mesh sampling on the AWT calculations.

As shown in Fig 2c), AWT was computed by: A) measuring the distance between each node in the epicardial surface and its nearest neighbor in the endocardial surface; B) repeating procedure A) in reverse for each node in the endocardial wall; C) averaging the outcomes of procedures A) and B). This method was first proposed for measurements of cortical thickness [35] and, in a comparative analysis of the precision of different algorithms to measure cortical thickness, was found to have the lowest variability of all the analyzed methods [36].

In each subject, AWT was encoded as a scalar field mapped to each vertex in the epicardial mesh. To allow direct comparisons with literature from other modalities, regions of interest (ROIs) were manually drawn in specific atrial regions and ROI-based AWT was estimated.

For vessel openings and the mitral and tricuspid valves, the nominal AWT was set to 0. These regions were not taken into account in the calculation of AWT statistics.

E Impact of Acquisition Resolution

To determine whether the image acquisition resolution (1.40 mm) could have introduced a bias in the AWT estimates, we imaged 2 volunteers at a higher resolution of 1.0 mm, using the scanning sequence described previously (scan time with a 100% breathing efficiency: 15 min). These images were processed as described above to create AWT maps.

The average of nearest neighbors method was also used to calculate the AWT of the widely-used Visible Female atrial geometry, created from the segmentation of 0.33-mm resolution photographs of cryosections of a female cadaver [37], [38]. Cryosectioning has been a cornerstone of cardiac morphology studies, enabling the reconstruction of even very fine details of the cardiac anatomy (e.g. [39]). We therefore compared the AWT estimated using this dataset and the acquired MR images as a further test for the impact of the acquisition resolution on AWT estimates.

F Atlas Creation

To create an AWT atlas, epicardial meshes from all volunteers were manually aligned and then non-linearly registered to the reconstructed atrial surface that was deemed to be closest

to the average atrial shape through visual inspection. The registration was performed with the snreg tool of the Image Registration Toolkit (https://www.doc.ic.ac.uk/~dr/software/). snreg models the non-rigid transformation between two meshes using a free-form deformation between each vertex of the source mesh and the nearest target vertex.

For each vertex of the target image, AWT was computed by averaging the AWT values in the matching vertices of the epicardial meshes of each of the imaged subjects using Matlab. The uncertainty in AWT computations was estimated, on a vertex-by-vertex basis, using the standard deviation of AWT across all subjects. Patient scans were not used as inputs to the AWT atlas.

III Results

A Imaging and Atrial Wall Thickness Maps

Fig. 3 shows three orthogonal views from typical PSIR images and the atrial wall segmentations. It can be observed that blood has a very low intensity, whereas myocardium appears hyperintense and is clearly distinguishable from both blood and surrounding non-cardiac tissue. A similar contrast can be observed in the two patient scans (Fig. 4).

Fig. 4 shows typical AWT maps of the left atrium of the two scanned patients and Fig 5, maps of the LA and RA of two volunteers. Similar qualitative features can be seen in all AWT maps. In the volunteer maps, a high thickness in the terminal crest (TC) region and low AWT in the pulmonary vein (PV) sleeves can be observed. Note that a direct comparison of these features with patient datasets was not possible, as the clinically-compatible patient scans were focused on the left atrium, the main target for ablation.

The Dice coefficient for the segmentation of the LA of the 4 analyzed subjects was 0.68 ± 0.06 and the 50%-percentile modified Hausdorff distance was 0.7 ± 0.2 mm. These metrics are similar to those reported in a challenge of the segmentation of the LA blood pool [34].

We additionally found that halving the mean internode distance of the created meshes made the AWT calculation much more computationally intensive, but had little effect on the computed AWT, changing mean AWT by less than 4%.

B Atrial Wall Thickness Atlas

Fig. 6 shows the atlas created from the AWT maps of the 10 volunteers, above a map of the uncertainty of the AWT. Both sides of the atria were found to have a similar average thickness: measured AWT was 2.7 ± 0.7 mm (0.6–4.5 mm) in the right atrium (RA) and 2.4 ± 0.7 mm (0.7–4.3 mm) in the LA. Across different subjects, there was little variation in the measured thickness values in most regions (<1.0 mm). Several features are clearly identifiable: the terminal crest bundle appears as a region of increased thickness (3.5–4.2 mm), whereas the pulmonary veins (1.5–2.2 mm) were on average thinner than the atrial walls. The highest variation (<2.5 mm) was found in small regions around the left PVs, around the superior vena cava and at near the fundi of the left and right atrial appendages, which showed high inter-subject morphological variability.

C Atrial Wall Thickness in Patients

AWT values in the left atrium were 3.1 ± 1.3 mm and 2.6 ± 0.7 mm in patients 1 and 2 (Fig. 4, Table 1). The AWT values for patient 2 are similar to those obtained in volunteers, whereas patient 1, who suffered from mitral regurgitation and a markedly enlarged left atrial cavity, was found to have an increased left atrial AWT. The reconstructed thickness meshes for these patients are shown in Fig. 4.

D Comparison with Literature

Fig. 7 compares AWT values obtained in this study with available previous literature reports of thickness in selected corresponding regions. The obtained AWT measurements are in general in good agreement with studies using other modalities, which show a high degree of variability in themselves.

The posterior left atrial wall, a region commonly targeted in ablation procedures and located in close proximity to the esophagus, was thicker in its inferior region, as reported previously in the post-mortem literature [8], [10]. Our measurements for the thickness of the PVs were performed approximately 0.5 cm away from the ostia, to match previous studies [13], [15]. They are at the upper end of the range found in the literature and, as in the literature, reveal a higher thickness in the right PVs compared to the left ones [12], [13].

In the RA, AWT has been measured in fewer specific regions, the exception being the terminal crest, which was the thickest region of the atria, also in good agreement with post-mortem reports [9].

E Impact of Acquisition Resolution

The 1.0-mm resolution scan was unsuccessful in one of the volunteers, whose breathing efficiency was low (expected scan time: 42 min) and who experienced severe discomfort in the scanner. In the other extremely cooperative volunteer (actual scan time: 23 min), the measured AWT was 2.9 ± 1.1 mm, in good agreement with the 3.3 ± 1.2 mm obtained using the lower resolution scan in the same volunteer. The AWT of the Visible Female atrial model, also computed using the average of nearest neighbors method, was 2.7 ± 1.4 mm, in excellent agreement with the computed thickness for the AWT atlas (2.4 ± 0.8 mm).

IV Discussion

We present a novel contrast agent-free MRI protocol to acquire atrial wall thickness information in a 10-min free-breathing scan. We successfully employ this technique to create the first whole atria atlas of wall thickness from images of 10 healthy volunteers. We also acquire atrial wall thickness maps in 2 AF patients, thus demonstrating the protocol's clinical use.

A Image Acquisition and Processing

To the best of our knowledge, this is the first study that proposes an MRI-based *in vivo* measurement of atrial wall thickness. We could not therefore perform a direct comparison between the proposed protocol and other MRI sequences. The acquired images show a good

contrast between the atrial myocardium, blood and periatrial structures. The endo- and epicardial surfaces were manually segmented, as variations in the intensity of the atrial wall, blood and neighboring structures precluded the direct use of automatic segmentation techniques. Furthermore, in regions such as the LA-ascending aorta border, it can be difficult to distinguish between the atrial and aortic borders, leading to a higher uncertainty in the local AWT estimates.

Automatic segmentation is considerably harder to implement in MRI than in CT, as image intensity in MRI is not solely determined by tissues' intrinsic properties and is strongly spatially varying, due to effects such as spatial variations in coil sensitivities and local magnetic susceptibility. Further studies will explore the use of automatic segmentation techniques, such as the ones described in [34] or [40], to complement or replace the manual delineation of the endocardial surface performed in the current study.

B Atrial Wall Thickness Measurements

AWT was computed using an average of nearest neighbors method, which is computationally simple to implement and was previously successfully applied to measure cortical thickness [35], [36]. The cortex and the atrial wall share an irregular geometry that may lead to inaccurate thickness measurements if these are performed along a pre-defined plane. It is therefore reasonable to assume that a method that performs well when estimating cortical thickness will also give reliable measurements of atrial thickness. Given the lack of a gold-standard method for thickness computations, it is likely that choosing a different method to calculate thickness would produce slightly different estimates of AWT, particularly in high-curvature regions where different methods are likely to yield disparate thickness estimates [36].

Clinically acceptable scan times put a limit in the spatial resolution that can be employed. A 1.40-mm isotropic resolution was used in the current study as a balance between spatial resolution, signal to noise ratio and scan time. At this spatial resolution, the imaging of very thin atrial structures such as the distal portions of pulmonary veins or the pectinate muscles is very challenging. We nevertheless show that in the main portion of the atria, our AWT estimates agree with higher resolution scans. We were in particular able to image, in a very long scan, the atria of a particularly cooperative volunteer at a higher resolution of 1.0 mm. The obtained AWT values were comparable, suggesting that the chosen spatial resolution did not introduce detectable systematic errors in AWT estimates. This is corroborated by the good agreement of AWT with previous reports and with the 0.33-mm resolution Visible Female. The latter dataset comes from photographs of the cryosectioned atria of a cadaver, which is a standard method of *ex vivo* cardiac reconstruction [39]. However, direct comparisons with the current *in vivo* protocol are not straightforward. Further studies will explore the impact of imaging resolution on AWT measurements more quantitatively.

C Atrial Wall Thickness Atlas

The 10 volunteer AWT maps were non-linearly registered to create an AWT atlas. The atrial shape of the 10 subjects was qualitatively similar, with all subjects showing 4 independent PVs which joined the LA at similar locations. The obtained thickness values were in good

Europe PMC Funders Author Manuscripts

agreement with previous literature reports from post-mortem and CT studies. The reported wide range of AWT estimates (see Fig. 7) makes, nevertheless, direct comparisons difficult.

The volunteer AWT atlas can be a valuable input for computational studies of atrial pathologies, such as AF. The atlas could thus contribute to determine the role of atrial wall thickness in the dynamics and location of the abnormal electrical circuits underlying AF or help determine the amount of ablation energy that should be delivered at each location of the atrium. Furthermore, the atlas can also be used as a benchmark for future studies aiming to determine how factors such as disease, age or medical interventions can affect AWT.

We expect there to be a high morphological variation in LA among AF patients [41] and therefore did not attempt to add the reconstruction of the patients' LA to the AWT atlas.

D Atrial Wall Thickness in Patients

We additionally show that our technique can be successfully employed to image AF patients who are in sinus rhythm at the time of the scan (such as cardioverted AF patients or paroxysmal AF patients in sinus rhythm). In the current study, the patient without structural heart disease had an AWT was similar to that of volunteers (Table 1), with the other patient showing marked variations in AWT, which was in general higher than in the imaged volunteers.

The proposed technique is, at the moment, unlikely to have a high success rate in patients who are in AF or have a high rate at the time of scan. The main reason for this is the reduced and irregular R-R in these patients, not allowing sufficiently long inversion times to obtain a good blood-myocardium contrast. Modifications of the current technique to allow inversion pulse repetition over more than 2 cardiac cycles may allow the proposed technique to be extended to these patients. Furthermore, the variability of the heart rate in patients with AF may also cause image artefacts. Although arrhythmia rejection could be employed to mitigate these effects, it would likely greatly extend the scan time. To prevent acquisition times from becoming overly long, image acceleration techniques which allow higher acceleration factors compared to conventional parallel imaging, such as compressed sensing, may be employed.

Patient-specific findings are likely to be of interest for electroanatomical mapping and catheter ablation planning in AF patients. Moreover, both the AWT maps and atlas can be used for modelling atrial electrophysiology and mechanics, with the aim of establishing quantitative links between atrial structure and function and their change during the progression of atrial arrhythmias [42]. Ultimately, this could lead to an improved understanding the role of AWT in cardiac arrhythmias, including the genesis of the abnormal electrical activity sustaining AF, the morphology of abnormal atrial electrograms and the impairment of the atrial pump function.

V Conclusion

We used a black-blood PSIR protocol to obtain atrial wall thickness maps in 10 healthy volunteers and combined them to create the first wall thickness atlas for the entire atria. The

obtained AWT estimates are in good agreement with values from other modalities where available and provide baseline values of AWT against which pathology-induced alterations can be measured. Furthermore, the proposed scan can be easily appended to existing clinical MRI protocols to create subject-specific AWT maps, as demonstrated here in 2 patients. This technique can be of particular interest when imaging patients with progressive disease in the pre-ablation setting, potentially providing information for both patient stratification and guidance in catheter ablation procedures.

References

[1]. Whitaker J, Rajani R, Chubb H, Gabrawi M, Varela M, Wright M, Niederer S, O'Neill M. The role of myocardial wall thickness in atrial arrhythmogenesis. Europace. May.2016 i(7):euw014.

[2]. Camm A, Lip GYH, De Caterina R, Savelieva I, Atar D, Hohnloser SH, Hindricks G, Kirchhof P. 2012 focused update of the ESC Guidelines for the management of atrial fibrillation: an update of the 2010 ESC Guidelines for the management of atrial fibrillation. Eur Heart J. Nov; 2012 33(21):2719–47. [PubMed: 22922413]

[3]. Calkins H, Kuck KH, Cappato R, Brugada J, Camm AJ, Chen S-A, Crijns HJG, Damiano RJ, Davies DW, DiMarco J, Edgerton J, et al. 2012 HRS/EHRA/ECAS Expert Consensus Statement on Catheter and Surgical Ablation of Atrial Fibrillation: recommendations for patient selection, procedural techniques, patient management and follow-up, definitions, endpoints, and research trial design. Europace. Apr; 2012 14(4):528–606. [PubMed: 22389422]

[4]. Yamazaki M, Mironov S, Taravant C, Brec J, Vaquero LM, Bandaru K, Avula UMR, Honjo H, Kodama I, Berenfeld O, Kalifa J. Heterogeneous atrial wall thickness and stretch promote scroll waves anchoring during atrial fibrillation. Cardiovasc Res. Apr; 2012 94(1):48–57. [PubMed: 22227155]

[5]. Wi J, Mun H-S, Uhm J-S, Shim J, Kim JH, Pak H-N, Lee M, Joung B. Complex fractionated electrograms related to left atrial thickness. J Am Coll Cardiol. Mar.2013 61(10):E307.

[6]. Kuznetsova T, Herbots L, Richart T, D'hooge J, Thijs L, Fagard RH, Herregods M-C, Staessen JA. Left ventricular strain and strain rate in a general population. Eur Heart J. Aug; 2008 29(16): 2014–23. [PubMed: 18583396]

[7]. Bisbal F, Guiu E, Calvo N, Marin D, Berruezo A, Arbelo E, Ortiz-Pérez J, de Caralt TM, Tolosana JM, Borràs R, Sitges M, et al. Left atrial sphericity: a new method to assess atrial remodeling. Impact on the outcome of atrial fibrillation ablation. J Cardiovasc Electrophysiol. Jul; 2013 24(7):752–9. [PubMed: 23489827]

[8]. Platonov PG, Ivanov V, Ho SY, Mitrofanova L. Left atrial posterior wall thickness in patients with and without atrial fibrillation: data from 298 consecutive autopsies. J Cardiovasc Electrophysiol. Jul; 2008 19(7):689–92. [PubMed: 18284501]

[9]. Sánchez-Quintana D, Anderson RH, Cabrera Ja, Climent V, Martin R, Farré J, Ho SY, Sanchez-Quintana D, Sánchez-Quintana D, Anderson RH, Cabrera Ja, et al. The terminal crest: morphological features relevant to electrophysiology. Heart. Oct; 2002 88(4):406–411. [PubMed: 12231604]

[10]. Sánchez-Quintana D, Cabrera JA, Climent V, Farré J, de Mendonça MC, Ho SY, De Mendonça MC. Anatomic relations between the esophagus and left atrium and relevance for ablation of atrial fibrillation. Circulation. Sep; 2005 112(10):1400–1405. [PubMed: 16129790]

[11]. Hall B, Jeevanantham V, Simon R, Filippone J, Vorobiof G, Daubert J. Variation in left atrial transmural wall thickness at sites commonly targeted for ablation of atrial fibrillation. J Interv Card Electrophysiol. Nov; 2006 17(2):127–32. [PubMed: 17226084]

[12]. Ho SY, Sanchez-Quintana D, Cabrera Ja, Anderson RH. Anatomy of the left atrium: implications for radiofrequency ablation of atrial fibrillation. J Cardiovasc Electrophysiol. Nov; 1999 10(11): 1525–33. [PubMed: 10571372]

[13]. Ho SY. Architecture of the pulmonary veins: relevance to radiofrequency ablation. Heart. Sep; 2001 86(3):265–270. [PubMed: 11514476]

[14]. Deneke T, Khargi K, Müller K-M, Lemke B, Mügge A, Laczkovics A, Becker AE, Grewe PH. Histopathology of intraoperatively induced linear radiofrequency ablation lesions in patients with chronic atrial fibrillation. Eur Heart J. Sep; 2005 26(17):1797–803. [PubMed: 15855195]

[15]. Hassink RJ, Aretz HT, Ruskin JN, Keane D. Morphology of atrial myocardium in human pulmonary veins: A postmortem analysis in patients with and without atrial fibrillation. J Am Coll Cardiol. 2003; 42(6):1108–1114. [PubMed: 13678939]

[16]. Wolf CM, Seslar SP, den Boer K, Juraszek AL, McGowan FX, Cowan DB, Del Nido P, Triedman JK, Berul CI, Walsh EP. Atrial remodeling after the Fontan operation. Am J Cardiol. Dec; 2009 104(12):1737–42. [PubMed: 19962486]

[17]. Becker AE. Left atrial isthmus: anatomic aspects relevant for linear catheter ablation procedures in humans. J Cardiovasc Electrophysiol. Jul; 2004 15(7):809–12. [PubMed: 15250867]

[18]. Schwartzman D, Schoedel K, Stolz DB, Di Martino E. Morphological and mechanical examination of the atrial ‘intima’. Europace. Nov; 2013 15(11):1557–61. [PubMed: 23608029]

[19]. Beinart R, Abbara S, Blum A, Ferencik M, Heist K, Ruskin JN, Mansour M. Left atrial wall thickness variability measured by CT scans in patients undergoing pulmonary vein isolation. J Cardiovasc Electrophysiol. Nov; 2011 22(11):1232–6. [PubMed: 21615817]

[20]. Nakamura K, Funabashi N, Uehara M, Ueda M, Murayama T, Takaoka H, Komuro I. Left atrial wall thickness in paroxysmal atrial fibrillation by multislice-CT is initial marker of structural remodeling and predictor of transition from paroxysmal to chronic form. Int J Cardiol. Apr; 2011 148(2):139–47. [PubMed: 19906452]

[21]. Wi J, Lee H-J, Uhm J-S, Kim J-YY, Pak H-N, Lee M, Kim YJ, Joung B. Complex Fractionated Atrial Electrograms Related to Left Atrial Wall Thickness. J Cardiovasc Electrophysiol. Nov; 2014 25(August 2011):1141–1149. [PubMed: 24948440]

[22]. Park J, Park CH, Lee H-J, Wi J, Uhm J-S, Pak H-N, Lee M, Kim YJ, Joung B. Left atrial wall thickness rather than epicardial fat thickness is related to complex fractionated atrial electrogram. Int J Cardiol. Apr; 2014 172(3):e411–3. [PubMed: 24439855]

[23]. Lemola K, Sneider M, Desjardins B, Case I, Han J, Good E, Tamirisa K, Tsemo A, Chugh A, Bogun F, Pelosi F, et al. Computed tomographic analysis of the anatomy of the left atrium and the esophagus: implications for left atrial catheter ablation. Circulation. Dec; 2004 110(24): 3655–60. [PubMed: 15569839]

[24]. Imada M, Funabashi N, Asano M, Uehara M, Ueda M, Komuro I. Anatomical remodeling of left atria in subjects with chronic and paroxysmal atrial fibrillation evaluated by multislice computed tomography. Int J Cardiol. Jul; 2007 119(3):384–8. [PubMed: 17064785]

[25]. Hoffmeister PS, Chaudhry GM, Mendel J, Almasry I, Tahir S, Marchese T, Haffajee CI, Orlov MV. Evaluation of left atrial and posterior mediastinal anatomy by multidetector helical computed tomography imaging: relevance to ablation. J Interv Card Electrophysiol. Apr; 2007 18(3):217–23. [PubMed: 17516160]

[26]. Pan N-H, Tsao H-M, Chang N, Chen Y-J, Chen S-A. Aging dilates atrium and pulmonary veins: implications for the genesis of atrial fibrillation. Chest. Jan; 2008 133(1):190–6. [PubMed: 18187745]

[27]. Suenari K, Nakano Y, Hirai Y, Ogi H, Oda N, Makita Y, Ueda S, Kajihara K, Tokuyama T, Motoda C, Fujiwara M, et al. Left atrial thickness under the catheter ablation lines in patients with paroxysmal atrial fibrillation: insights from 64-slice multidetector computed tomography. Heart Vessels. May; 2013 28(3):360–8. [PubMed: 22526381]

[28]. Bishop MJ, Rajani R, Plank G, Gaddum N, Carr-White G, Wright M, O’Neill M, Niederer S. Three-dimensional atrial wall thickness maps to inform catheter ablation procedures for atrial fibrillation. Europace. 2016; 18(3):376–83. [PubMed: 25842272]

[29]. Kellman P, Arai AE, McVeigh E, Aletras A. Phase-sensitive inversion recovery for detecting myocardial infarction using gadolinium-delayed hyperenhancement. Magn Reson Med. 2002; 47:372–383. [PubMed: 11810682]

[30]. Yushkevich PA, Piven J, Hazlett HC, Smith RG, Ho SY, Gee JC, Gerig G. User-guided 3D active contour segmentation of anatomical structures: significantly improved efficiency and reliability. Neuroimage. Jul; 2006 31(3):1116–28. [PubMed: 16545965]

[31]. CIBC. Seg3D: Volumetric Image Segmentation and Visualization. Scientific Computing and Imaging Institute (SCI); 2016. Download from: http://www.seg3d.org

[32]. Fedorov A, Beichel R, Kalpathy-Cramer J, Finet J, Fillion-Robin J-C, Pujol S, Bauer C, Jennings D, Fennessy F, Sonka M, Buatti J, et al. 3D Slicer as an image computing platform for the Quantitative Imaging Network. Magn Reson Imaging. 2012; 30(9):1323–1341. [PubMed: 22770690]

[33]. Dubuisson, M-P., Jain, AK. A modified Hausdorff distance for object matching. Proceedings of 12th International Conference on Pattern Recognition; p. 566-568.

[34]. Tobon-Gomez C, Geers AJ, Peters J, Weese J, Pinto K, Karim R, Ammar M, Daoudi A, Margeta J, Sandoval Z, Stender B, et al. Benchmark for Algorithms Segmenting the Left Atrium From 3D CT and MRI Datasets. IEEE Trans Med Imaging. Jul; 2015 34(7):1460–1473.

[35]. Fischl B, Dale AM. Measuring the thickness of the human cerebral cortex from magnetic resonance images. Proc Natl Acad Sci U S A. Sep; 2000 97(20):11050–5. [PubMed: 10984517]

[36]. Lerch JP, Evans AC. Cortical thickness analysis examined through power analysis and a population simulation. Neuroimage. Jan; 2005 24(1):163–73. [PubMed: 15588607]

[37]. Ackerman MJ. The Visible Human Project. Proc IEEE. Mar; 1998 86(3):504–511.

[38]. Freudenberg J, Schiemann T, Tiede U, Höhne KH. Simulation of cardiac excitation patterns in a three-dimensional anatomical heart atlas. Comput Biol Med. Jul; 2000 30(4):191–205. [PubMed: 10821938]

[39]. Dobrzynski H, Li J, Tellez J, Greener ID, Nikolski VP, Wright SE, Parson SH, Jones SA, Lancaster MK, Yamamoto M, Honjo H, et al. Computer Three-Dimensional Reconstruction of the Sinoatrial Node. Circulation. 2005; 111(7)

[40]. Koppert, MMJ., Rongen, PMJ., Prokop, M., ter Haar Romeny, BM., van Assen, HC. Cardiac left atrium CT image segmentation for ablation guidance. 2010 IEEE International Symposium on Biomedical Imaging: From Nano to Macro; 2010. p. 480-483.

[41]. Varela M, Bisbal F, Zacur E, Berruezo A, Aslanidi O, Mont L, Lamata P. Novel computational analysis of left atrial anatomy improves prediction of atrial fibrillation recurrence after ablation. Front Physiol. 2017; 8:68. [PubMed: 28261103]

[42]. Morgan R, Colman MA, Chubb H, Seemann G, Aslanidi OV. Slow Conduction in the Border Zones of Patchy Fibrosis Stabilizes the Drivers for Atrial Fibrillation: Insights from Multi-Scale Human Atrial Modeling. Front Physiol. Oct.2016 7:474. [PubMed: 27826248]

Europe PMC Funders Author Manuscripts

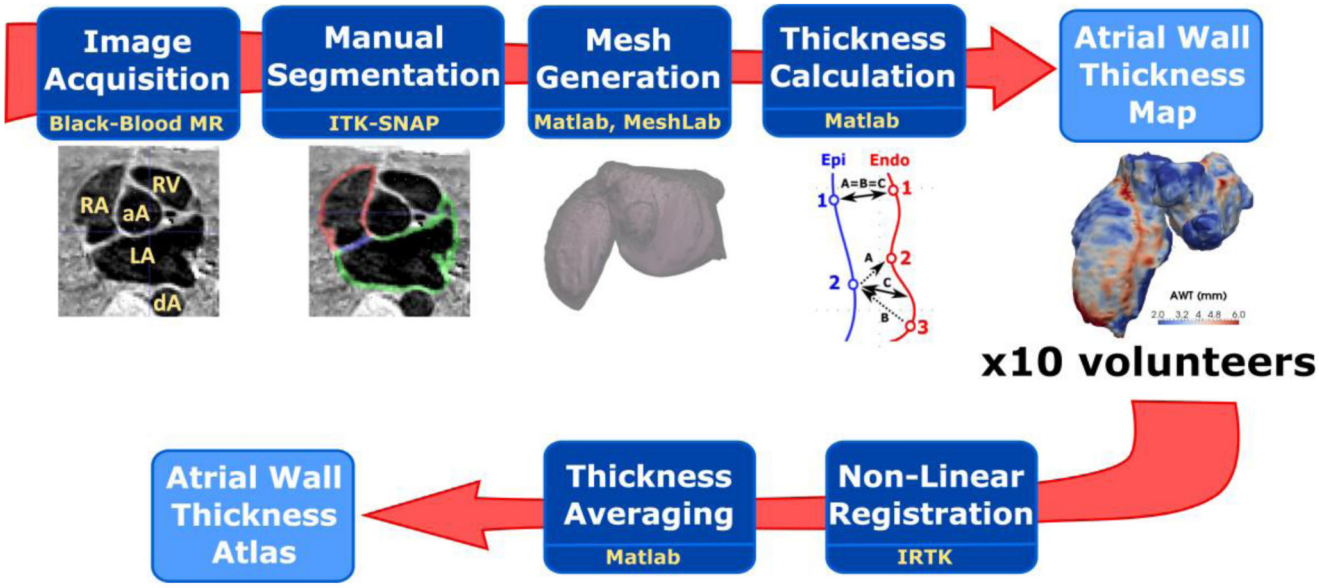

Fig. 1.

Pipeline of the processes used to create atrial wall thickness maps for each subject (top row) and to create an atrial wall thickness atlas (bottom row). aA: ascending aorta; dA: descending aorta; LA: left atrium; RV: right ventricle; RA: right atrium.

Europe PMC Funders Author Manuscripts

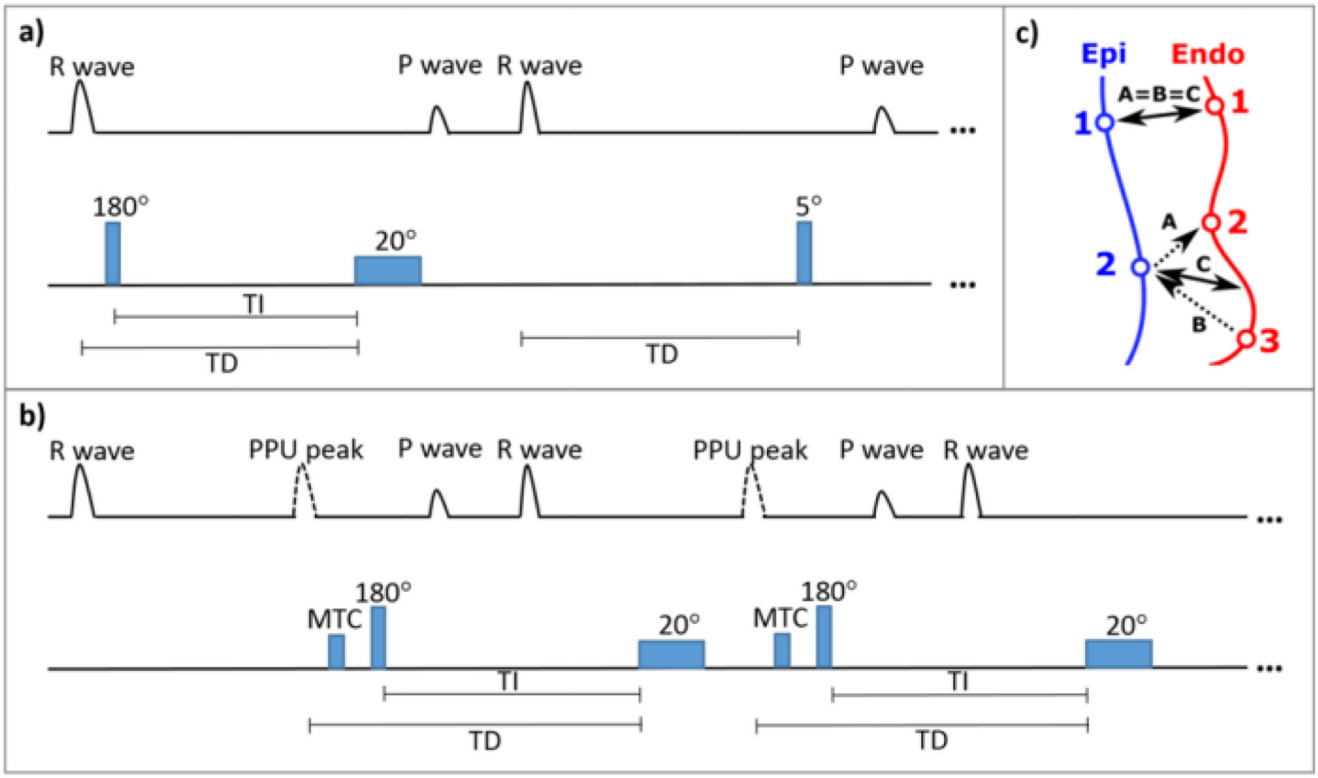

Fig. 2.

a) Pulse sequence diagram, over two cardiac cycles, of the PSIR sequence used in volunteers. Every other heartbeat, a non-selective inversion pulse (180°) is played an inversion time TI before the beginning of the 3D FLASH image readout (flip angle: 20°), which is timed to late atrial diastole (before the P wave). In the following cardiac cycle, no inversion is performed, but a low-contrast reference image (flip angle: 5°) is acquired at the same trigger delay, TD. b) Pulse sequence diagram, over two cardiac cycles, of the sequence used in patients. Here, the 180°/5° pulse is triggered by the PPU pulse peak and preceded by a magnetization transfer contrast (MTC) pulse to partially saturate the signal from the myocardium. c) Diagram illustrating the average of nearest neighbors method used to determine atrial wall thickness. For every vertex in the epi-/endocardial mesh, the corresponding nearest neighbor in the endo-/epicardial mesh is identified. The average distance between nearest-neighbor pairs (“C” in the diagram) is assigned to the corresponding epicardial mesh vertex to generate the AWT map.

Europe PMC Funders Author Manuscripts

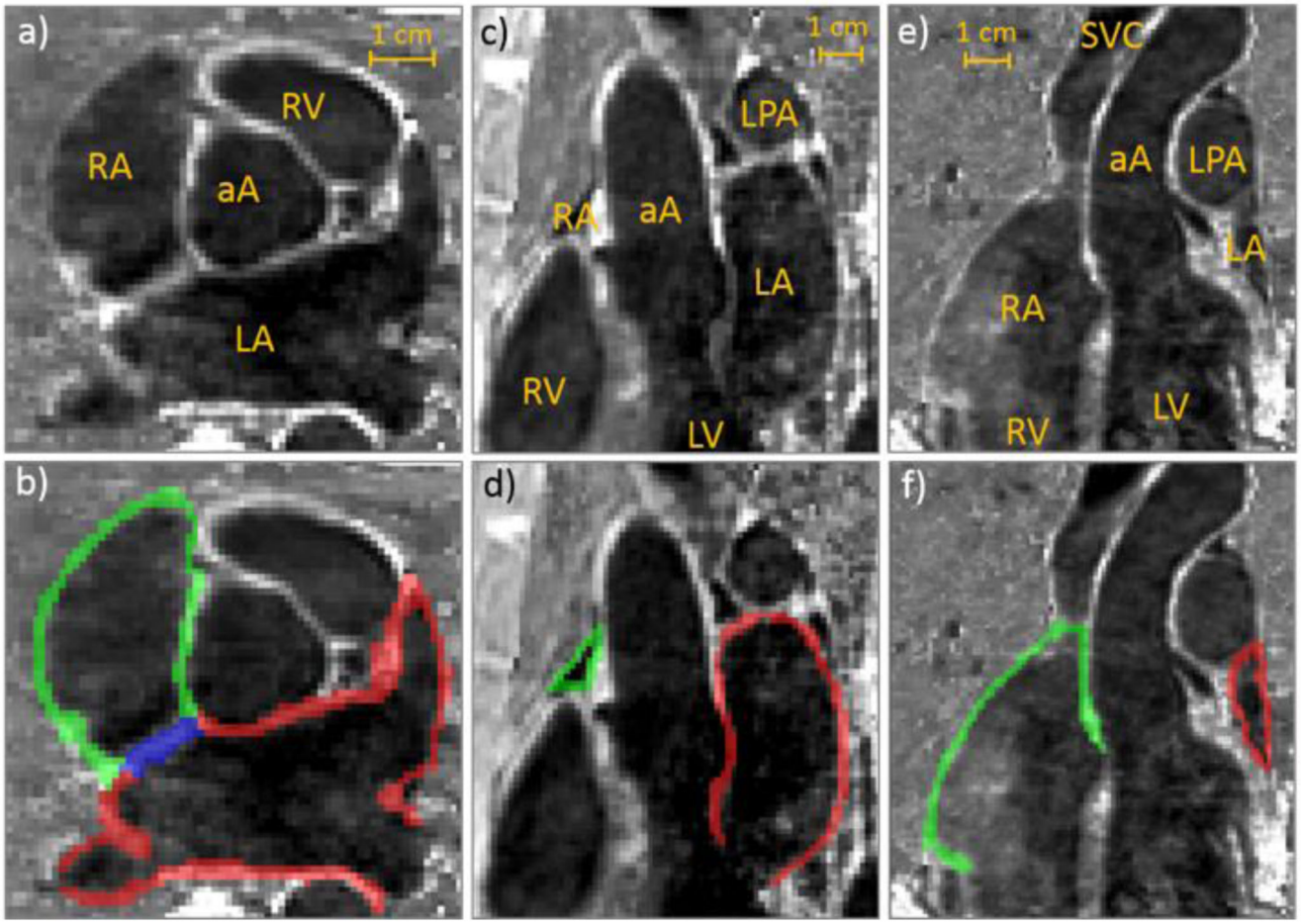

Fig. 3.

a, b) Axial, c, d) sagittal and e, f) coronal views of the atria from one representative subject overlaid, in the bottom row, with the performed manual segmentations. Green: right atrial wall; red: left atrial wall and blue: atrial septum. aA: ascending aorta; LA: left atrium; LPA: left pulmonary artery; LV: left ventricle; RA: right atrium; RV: right ventricle; SVC: superior vena cava.

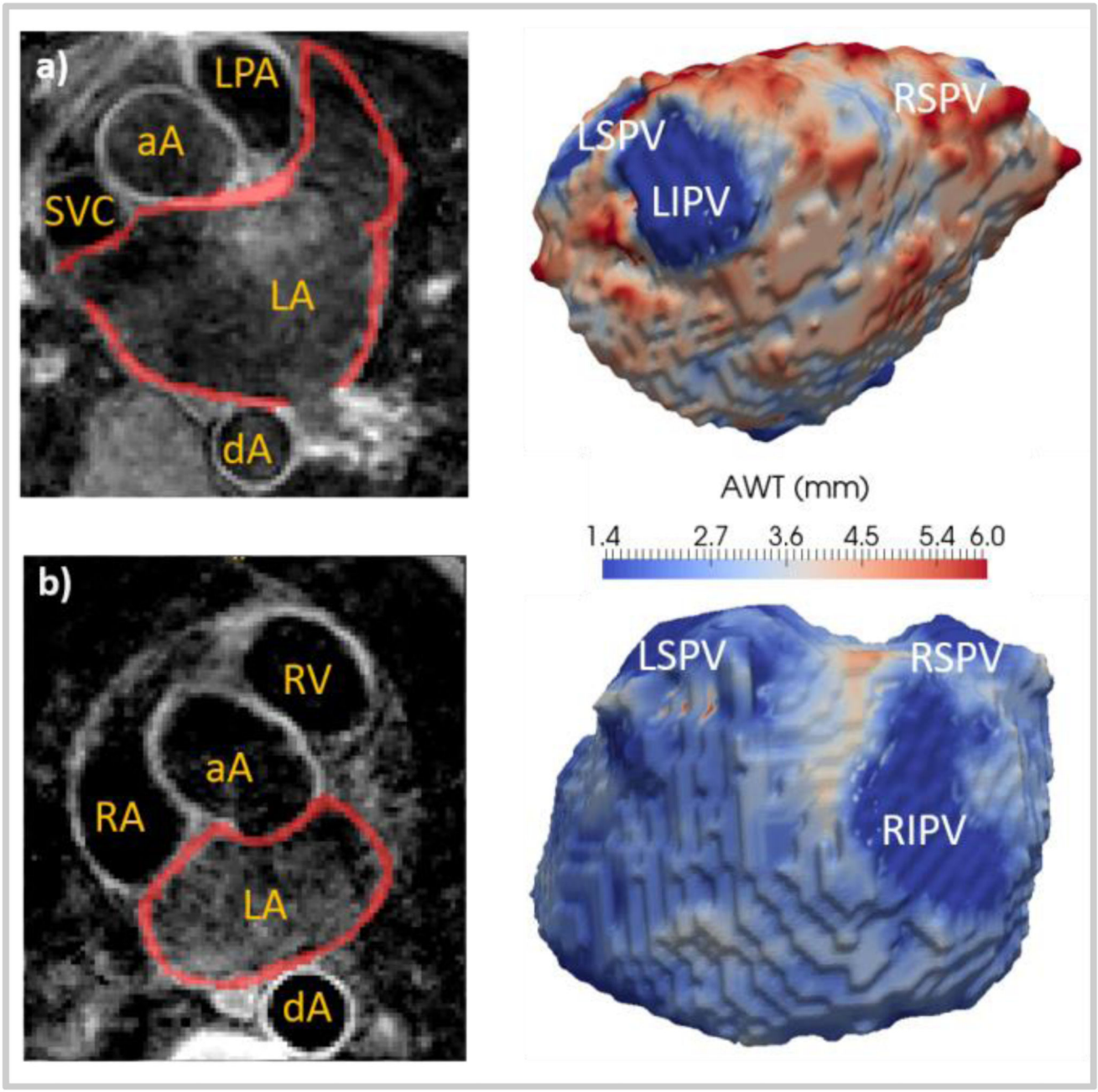

Fig. 4.

Left atrial axial view overlaid with the performed manual segmentations (left) and left atrial thickness maps (AWT, right) for: a) patient 1 and b) patient 2. Patient characteristics are described in Table 1. The abbreviations used are the same as in Figs. 3 and 5.

Europe PMC Funders Author Manuscripts

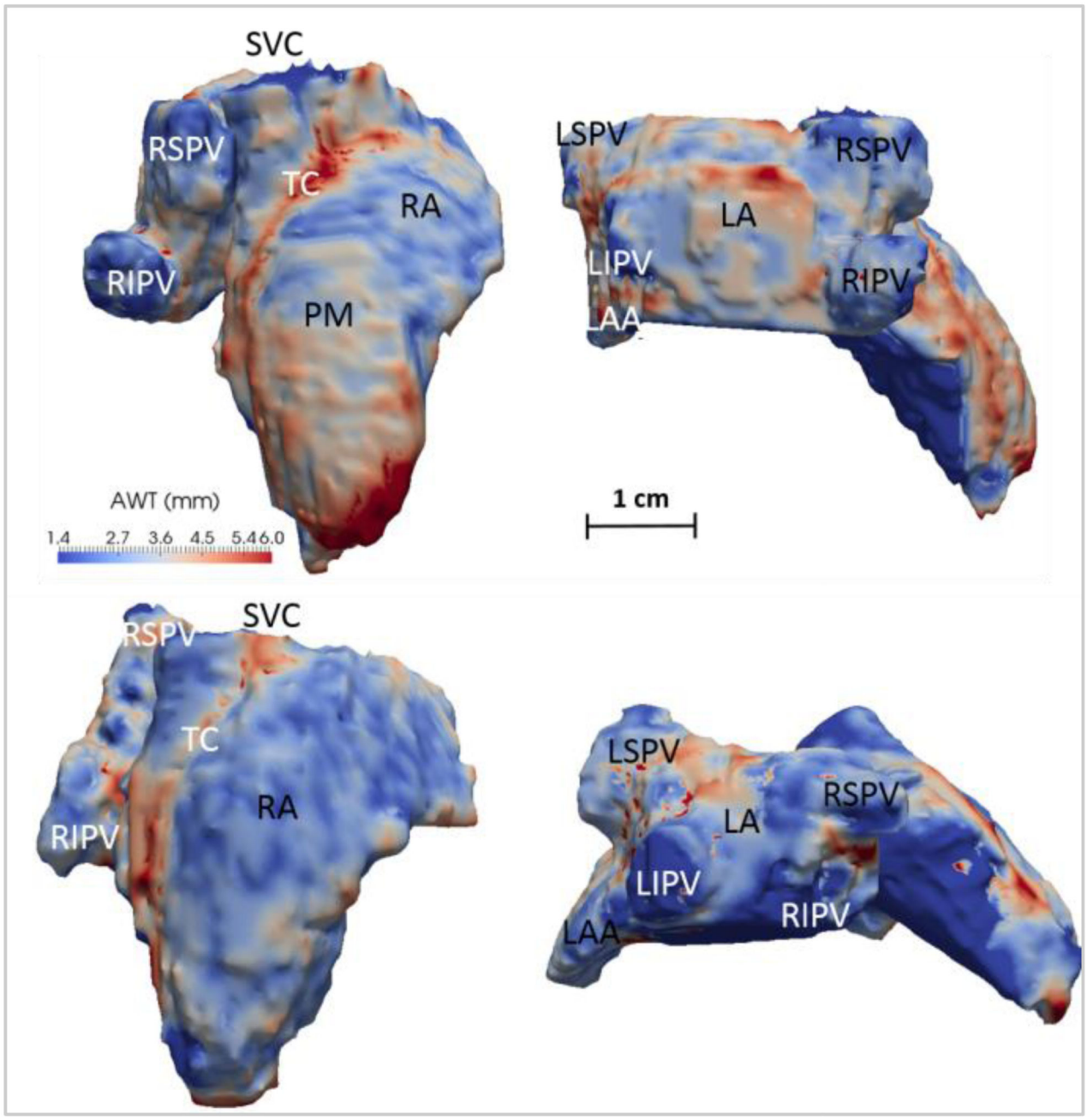

Fig. 5.

Atrial thickness maps from two different subjects (top and bottom)in: a right view (left) and a posterior view (right). RA: Right Atrium; LA: Left Atrium; LAA: Left Atrial Appendage; PV: Pulmonary Vein - RS: Right Superior; LS: Left Superior; RI: Right Inferior; LI: Left Inferior; SVC: Superior Vena Cava; TC: Terminal Crest (Crista Terminalis). In the top subject, the pectinate muscles (PMs) can be observed on the anterior RA wall emanating perpendicularly to the TC. The colour and distance scales are the same for both subjects.

Europe PMC Funders Author Manuscripts

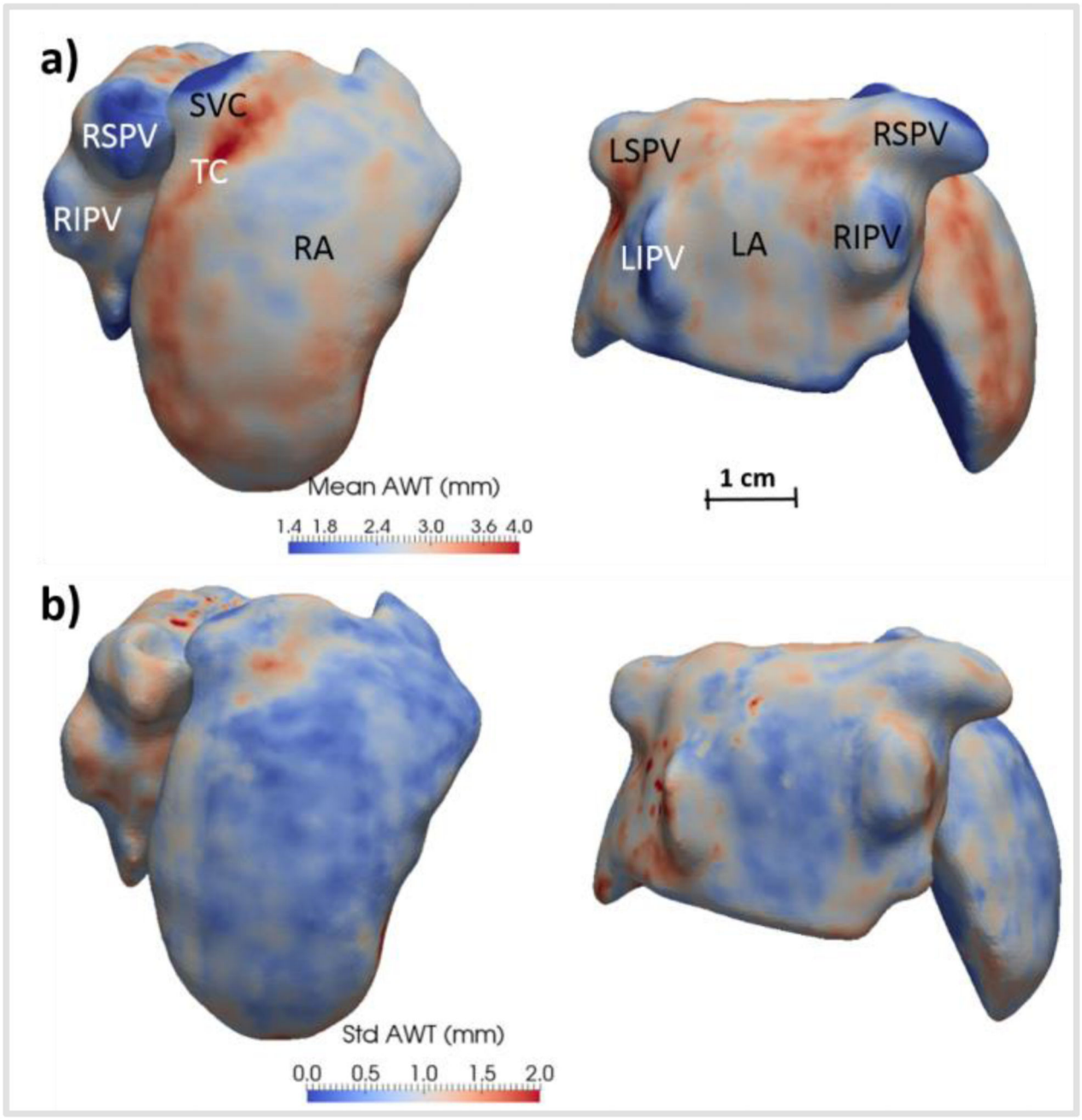

Fig. 6.

a) Atlas of atrial wall thickness (AWT) created from 10 healthy subjects in right (left panel) and posterior views (right panel). b) Uncertainty in AWT in the atlas, computed as the standard deviation across each subject for each data point. The abbreviations used are the same as in Fig. 5.

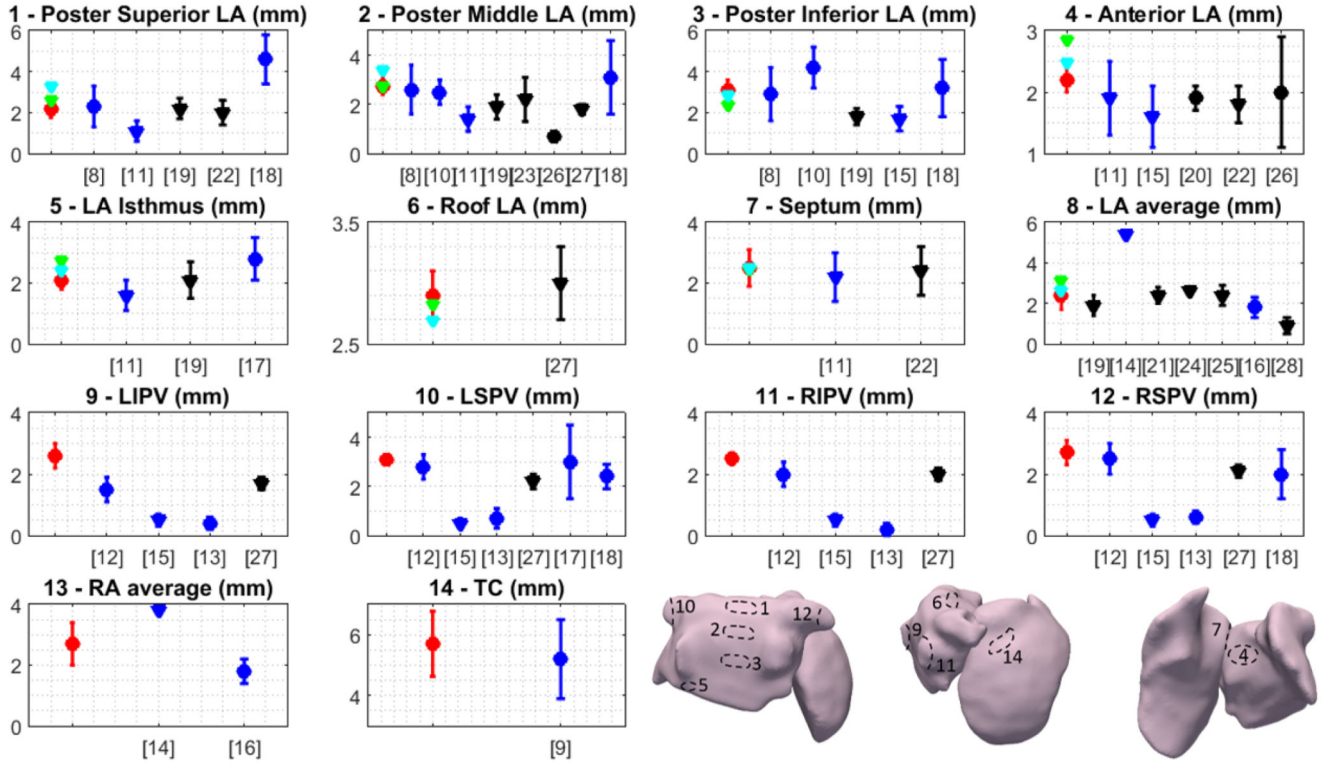

Fig. 7.

Atrial wall thickness measured in several regions in the current MRI study in volunteers (red), Patient 1 (green) and Patient 2 (light blue), alongside literature measurements using CT (black) or post-mortem studies (dark blue). Measurements in subjects who had no cardiac pathology/some form of cardiac pathology are represented by circles/triangles, respectively. References for each of the literature studies are shown in square brackets. The abbreviations used are the same as in Fig. 5 and each of the numbered regions is schematically depicted in the bottom right corner of the figure.

Europe PMC Funders Author Manuscripts

Europe PMC Funders Author Manuscripts

Table 1

Patient Scans

Clinical details of the two scanned patients, accompanied by the obtained atrial wall thickness values in the left atrium (mean ± standard deviation).

#	Age	Gender	Clinical Details	LA AWT (mm)
1	32	M	Paroxysmal AF, prosthetic (tissue) mitral valve replacement, 1 previous surgical ablation, 2 previous catheter ablations	3.1 ± 1.3
2	74	F	Paroxysmal AF, hypertension, 1 previous cardioversion, no previous ablations	2.6 ± 0.7